

Bifurcations in the Kuramoto model with external forcing and higher-order interactions

Guilherme S. Costa¹, Marcel Novaes^{2,3}, and Marcus A. M. de Aguiar^{1,3}

¹ *ICTP South American Institute for Fundamental Research & Instituto de Física Teórica - UNESP, 01140-070, São Paulo, Brazil*

² *Instituto de Física, Universidade Federal de Uberlândia, 38408-100, Uberlândia, MG, Brazil and*

³ *Instituto de Física Gleb Wataghin, Universidade Estadual de Campinas, 13083-970, Campinas, SP, Brazil*

Synchronization is an important phenomenon in a wide variety of systems comprising interacting oscillatory units, whether natural (like neurons, biochemical reactions, cardiac cells) or artificial (like metronomes, power grids, Josephson junctions). The Kuramoto model provides a simple description of these systems and has been useful in their mathematical exploration. Here we investigate this model in the presence of two characteristics that may be important in applications: an external periodic influence and higher-order interactions among the units. The combination of these ingredients leads to a very rich bifurcation scenario in the dynamics of the order parameter that describes phase transitions. Our theoretical calculations are validated by numerical simulations.

I. INTRODUCTION

In a seminal paper published in 1975, Kuramoto showed that non-linear oscillators with a stable limit cycle could synchronize their motion if the mutual interactions were sufficiently weak [1]. In his model, the oscillators were characterized by a single variable, describing the phase along the cycle, and pairwise interactions were approximated by smooth functions of the phase difference between the oscillators [2–4]. Kuramoto showed that synchronization would occur only if the coupling strength was larger than a minimum value, and would increase smoothly for larger coupling intensities, as in a continuous phase transition.

The Kuramoto model has become a paradigm in the field of synchronization and has been explored and extended in many directions since its inception [5]. Examples are the introduction of frustration [6], networks of connections and different distributions of the oscillator's natural frequencies [7–9] and multi-dimensional models [10–13]. One particularly important, and largely overlooked extension, considers the dynamics of periodically forced oscillators, where mutual synchronization competes with forced entrainment [14–16]. In many biological and artificial systems synchronization can indeed be strongly affected by external stimuli. It is well known that photo-sensitivity to flashing lights can trigger epileptic seizures [17] and that artificial pacemakers can control synchronization of heart cells [18]. Information processing in the brain can also be triggered by visual, auditory or olfactory inputs [19]. The visual cortex, in particular, exhibits different patterns of synchronized neuronal firing when subjected to stimuli [20].

This model considers N oscillators described by their phases and interacting with each

other according to

$$\dot{\theta}_i = \omega_i + \frac{K}{N} \sum_{j=1}^N \sin(\theta_j - \theta_i), \quad (1)$$

where K is a coupling constant and the natural frequencies ω_i are drawn at random from a distribution $g(\omega)$ of mean ω_0 and unit variance (this can always be achieved by a proper scaling of the variables). It has been shown that a phase transition exists in the large- N limit, with oscillators becoming synchronized as soon as K is larger than some critical value K_c that depends on $g(\omega)$. The transition may be of first or of second order, again depending on $g(\omega)$.

The introduction of an external forcing, acting on each oscillator as $F \sin(\sigma t - \theta_i)$, is an important extension of the original Kuramoto model [14, 21–23]. This corresponds to an overall influence of the environment upon the system. It creates a tendency to synchronize at the frequency σ , and therefore competes with the internal dynamics if $\sigma \neq \omega_0$. This problem was studied by Childs and Strogatz [14], who found that the asymptotic state can undergo several phase transitions as the parameters F and $\Omega = \sigma - \omega_0$ are varied. Concretely, they have found explicit formulas for the boundaries between different phases in the (F, Ω) plane. These boundaries are bifurcation curves, which may be of Hopf, saddle-node, SNIPER (saddle-node with infinite period) or homoclinic type.

More recently, attention has shifted to the effects of higher order interactions in systems of coupled oscillators [24]. In many complex systems, interactions go beyond pairwise terms, and involve the simultaneous action of groups of agents. Examples can be found in neuroscience [25–29], ecology [30, 31], biology [32] and social sciences [33, 34]. Studies have shown that the inclusion of higher order interactions have important consequences in the propagation of epidemics [35–37] and synchronization [38–45].

Pairwise, or two-body, interactions corresponds to the notion of an “interaction graph”. For higher order interactions this concept is replaced by that of a simplicial complex or hypergraphs which, besides nodes and edges, also contains triangles, tetrahedra, etc. This is usually done by the addition, in the Kuramoto equation for $\dot{\theta}_i$, of interaction terms proportional to $K_2 \sin(2\theta_j - \theta_k - \theta_i)$ and $K_3 \sin(\theta_j + \theta_k - \theta_m - \theta_i)$. In such a way each oscillator is allowed to interact with two or three of its neighbours simultaneously, in a way which is not reducible to two-body terms. These particular types of interactions were investigated by Skardal and Arenas [40], who showed that, if the higher-order interactions are strong enough, they can lead to bi-stability and the appearance of a first-order phase transition. The corresponding bifurcation diagram, which contains a saddle-node line and a pitchfork line, was also discussed in this work.

Here we bring together the two generalizations discussed above, treating a Kuramoto system which is subject to an external influence and whose internal dynamics contains higher-order terms of the form considered in [40]. It turns out that, as already observed in previous works, the dynamics of the system depends on K_2 and K_3 only through their sum, $K_{23} = K_2 + K_3$. Exploring the dynamics in full detail on the four-dimensional space of parameters (K_1, K_{23}, F, Ω) is impractical, so we develop two approaches: we investigate the

effect of K_{23} on the bifurcation diagram of the forced system, and the effect of the forcing on the bifurcation diagram of the simplicial system.

We find that any positive amount of forcing changes the nature of the pitchfork curve on the (K_1, K_{23}) plane, turning it into a saddle-node curve. Moreover, the bifurcation curves are changed in such a way that with increasing forcing the bi-stability region shrinks and eventually disappears for a critical value of F . On the other hand, the influence of K_{23} on the bifurcation curves on the (F, Ω) plane is even more dramatic. In particular, all bifurcation curves are doubled if $K_1 < 2$ and K_{23} is larger than some critical value.

II. THE MODEL

We consider the problem of a Kuramoto model where oscillators interact in all possible pairs, triplets and quadruples, and are also subject to a periodic external force

$$\begin{aligned} \dot{\theta}_i = & \omega_i + \frac{K_1}{N} \sum_{j=1}^N \sin(\theta_j - \theta_i) + \frac{k_2}{N^2} \sum_{j,k=1}^N \sin(2\theta_j - \theta_k - \theta_i) \\ & + \frac{k_3}{N^3} \sum_{j,k,m=1}^N \sin(\theta_j + \theta_k - \theta_m - \theta_i) + F \sin(\sigma t - \theta_i), \end{aligned} \quad (2)$$

where K_1 is the usual coupling constant, while k_2 and k_3 are new coupling constants that control the relative intensity of 2-simplexes and 3-simplexes, respectively. The natural frequencies ω_i are still drawn at random from a distribution $g(\omega)$ of mean ω_0 and unit variance. The particular form of higher order interactions described above is the same as in [40] and we refer to it as *asymmetric* because of the way θ_i enters the equations. *Symmetric* higher order interactions have also been considered [39, 41] but we shall not discuss them here.

We now introduce two order parameters

$$z = r e^{i\psi} \equiv \frac{1}{N} \sum_{i=1}^N e^{i\theta_i}, \quad (3)$$

and

$$z_2 = \frac{1}{N} \sum_j e^{2i\theta_j} \equiv r_2 e^{i\psi_2}, \quad (4)$$

and change variables to $\theta'_i = \theta_i - \sigma t$, i.e. to a coordinate system that is rotating with the same frequency of the external influence. In these new coordinates, after dropping the primes, we obtain

$$\dot{\theta}_i = (\omega_i - \sigma) + K_1 r \sin(\psi - \theta_i) + k_2 r r_2 \sin(\psi_2 - \theta_i - \psi) + k_3 r^3 \sin(\psi - \theta_i) - F \sin(\theta_i). \quad (5)$$

Let $f(\theta, \omega, t)$ be the density of oscillators, in the $N \rightarrow \infty$ limit, with natural frequency ω and phase θ at time t , so that $\int_0^{2\pi} f(\theta, \omega, t) d\theta = g(\omega)$. Using a continuity equation, the

infinite system of equations of motion for the phases can be turned into an infinite system of equations of motion for the Fourier modes of f ,

$$f = \frac{g(\omega)}{2\pi} \left(1 + \sum_{n=1}^{\infty} f_n e^{in\theta} + c.c. \right). \quad (6)$$

Upon introducing the well known Ott-Antonsen ansatz,

$$f_n = [\alpha(\omega, t)]^n, \quad (7)$$

this system collapses into two equations, namely

$$\dot{\alpha} = \frac{1}{2}(H^* + F) + i(\sigma - \omega)\alpha - \frac{1}{2}(H + F)\alpha^2, \quad (8)$$

and

$$z = \int g(\omega)\alpha(\omega)d\omega, \quad (9)$$

where

$$H = K_1 z + k_2 z_2 z^* + k_3 z^2 z^*. \quad (10)$$

We now assume that $g(\omega)$ is a Lorentzian distribution centered on ω_0 and with unit width $\Delta = 1$. This allows for analytic calculations, although numerical solutions indicate that this is not essential and the main results are good approximations when other distributions with infinite support, like Gaussians, are involved. The Lorentzian assumption allows the integration to be performed by residues, in which case we have that $z_2 = z^2$ and only one order parameter is required to describe the evolution of the system in the thermodynamic limit. This also means that $H = K_1 z + (k_2 + k_3)z|z|^2$, so only the sum of the coupling constants k_2 and k_3 is important.

This leads to a pair of coupled equations for the modulus and phase of the order parameter:

$$\dot{r} = -r + \frac{r}{2}(1 - r^2)(K_1 + K_{23}r^2) + \frac{F}{2}(1 - r^2)\cos\psi \equiv a(r, \psi) \quad (11)$$

and

$$\dot{\psi} = -\Omega - \frac{F}{2} \left(r + \frac{1}{r} \right) \sin\psi \equiv b(r, \psi). \quad (12)$$

where $K_{23} = k_2 + k_3$ and

$$\Omega = \sigma - \omega_0. \quad (13)$$

The roots to the above equations, $a(r_0, \psi_0) = 0$, $b(r_0, \psi_0) = 0$, are equilibrium points of the order parameter dynamics, which may be stable or unstable. Depending on the parameters, the dynamics may be structured around cycles, with vanishing a and constant b , and these may be attracting or repelling. Moreover, equilibrium points and cycles may

be created and destroyed in bifurcations as the parameters are varied. Local information can be obtained from the Jacobian matrix,

$$J = \begin{pmatrix} \frac{\partial a}{\partial r} & \frac{\partial a}{\partial \psi} \\ \frac{\partial b}{\partial r} & \frac{\partial b}{\partial \psi} \end{pmatrix}. \quad (14)$$

A complete characterization of the dynamics in the four-dimensional space of parameters (K_1, K_{23}, F, Ω) is impractical, so in the next sections we investigate the possible bifurcation scenarios under the effect of F, Ω with K_1, K_{23} fixed, and under the effect of K_1, K_{23} with F, Ω fixed. We restrict our attention to positive values of all parameters.

III. SIMPLICIAL PARAMETERS AS FIXED

We consider K_1 and K_{23} as given fixed parameters, and the forcing parameters F and Ω as being variables. Our calculations are similar to the ones done in [14], which considered only the case $K_{23} = 0$.

A. Saddle-Node bifurcations

Saddle-node (SN) bifurcations are characterized by one of the eigenvalues of the Jacobian being zero at the equilibrium solutions (r_0, ψ_0) . The bifurcation manifold is thus determined by the equations $a(r_0, \psi_0) = 0$, $b(r_0, \psi_0) = 0$, and $\det[J(r_0, \psi_0)] = 0$. Solving these for F , Ω and ψ leads to parametric equations in terms of the order parameter r :

$$F_{\text{SN}} = \sqrt{\frac{2}{1-r^2}} AB r^2, \quad (15)$$

$$\Omega_{\text{SN}} = \sqrt{\frac{(1+r^2)^3}{1-r^2}} 2AC, \quad (16)$$

and

$$\tan(\psi_{\text{SN}}) = \sqrt{\frac{1+r^2}{1-r^2}} \frac{C}{A}, \quad (17)$$

where

$$A = \sqrt{m - K_1 - K_{23}r^2}, \quad (18)$$

$$B = \sqrt{-m^2 + K_1 + K_{23}(1+2r^2)}, \quad (19)$$

$$C = \sqrt{K_1 + 3K_{23}r^2 - m \frac{1+r^2}{1-r^2}}, \quad (20)$$

and $m = 2/(1-r^2)$.

B. Hopf bifurcations

Hopf bifurcations requires the eigenvalues to be of the form $\pm i\omega$ at the bifurcation point. Therefore we impose $\text{tr}(J) = 0$ and $\det(J) > 0$. We will deal with this last condition later. This bifurcation manifold is determined by $a(r_0, \psi_0) = 0$, $b(r_0, \psi_0) = 0$ and $\text{Tr}[J(r_0, \psi_0)] = 0$. They can be written, after some simplification, as

$$K_1 = \frac{2}{1-r^2} - \frac{F}{r} \cos \psi - K_{23}r^2, \quad (21)$$

$$\frac{F}{r} \sin \psi = -\frac{2\Omega}{1+r^2} \quad (22)$$

and

$$\frac{F}{r} \cos \psi = \frac{1}{1+3r^2} [K_1(1-3r^2) - 2 + r^2 K_{23}(3-5r^2)]. \quad (23)$$

Using (21) and (23) to eliminate $F \cos \phi$ we get

$$K_1 = \frac{2(1+r^2)}{1-r^2} - K_{23}r^2(2-r^2). \quad (24)$$

This equation can be solved to get $r_{\text{Hopf}}(K_1, K_{23})$. Notice that there is in general more than one solution. When $K_{23} = 0$ we find, in agreement with [14],

$$r_{\text{Hopf}} = \sqrt{(K_1 - 2)/(K_1 + 2)}. \quad (25)$$

Squaring Eqs. (22) and (23) and adding them, we obtain, after some simplifications,

$$F_{\text{Hopf}} = r_{\text{Hopf}} \left\{ \frac{4\Omega^2}{(1+r_{\text{Hopf}}^2)^2} + \frac{r_{\text{Hopf}}^4}{(1-r_{\text{Hopf}}^2)^2} [2 - K_{23}(1-r_{\text{Hopf}}^2)^2] \right\}^{1/2} \quad (26)$$

Notice that for large Ω the plot of $F(\Omega)$ can be approximated by a straight line (when $K_{23} = 0$ the above expression reduces to the corresponding one in [14]).

The Hopf bifurcation requires $\det(J) > 0$. The point where $\det(J) = 0$ is where the Hopf curve meets the saddle-node curve. This is called the Takens-Bogdanov (TB) point. The value of Ω where this occurs is given by Eq.(16) computed at $r_{\text{Hopf}}(K_1, K_{23})$.

When $K_{23} \neq 0$, Eq.(24) has to be solved numerically, considering real roots in the interval $0 < r < 1$. For $K_1 > 2$ there is always one root. For $K_1 < 2$ the plot of K_{23} as a function of r is U-shaped and there are two roots if K_{23} is larger than the critical value K_{23}^* , where $\partial K_{23}/\partial r = 0$. The roots correspond to the two Hopf curves displayed in Fig. 1. At K_{23}^* the two roots coalesce and disappear together with the Hopf bifurcations. For instance, when $K_1 = 1$ we find $K_{23}^* = 5.306$.

C. Example: $K = 1$ and $K_{23} = 7$

Figure 1 shows the saddle-node and Hopf curves for $K = 1$ and $K_{23} = 7$. A dramatic difference with the case $K_{23} = 0$ is that there are now two bifurcation ‘‘tongues’’ where there

was previously only one: we find two saddle-node curves, two SNIPER curves and two Hopf curves. When $K_{23} = 0$ (only pairwise interactions) all these bifurcation manifolds exist only for $K_1 > 2$, as can be seen from Eq.(25). That means that in the absence of forcing and higher order interactions the system recovers the Kuramoto model, which synchronizes only if $K_1 > 2$ for Lorentzian distributions with $\Delta = 1$. In the next section we discuss the limit of small forcing with higher order interactions. Figure 1(b) shows a heat map of the time averaged order parameter r , showing very clearly the phase transitions that take place as one crosses the bifurcation lines.

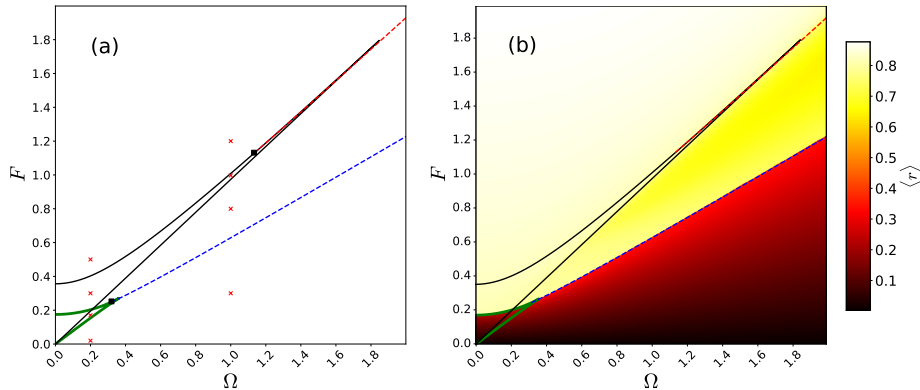


Figure 1. (a) Saddle-node bifurcation (thin black and thick green solid lines) and Hopf curves (red and blue dashed lines) in the $F \times \Omega$ plane for $K_1 = 1$ and $K_{23} = 7$. Red points correspond to phase diagrams in figure 2. Black squares are Takens-Bogdanov bifurcation points, where the Hopf and saddle-node lines meet. (b) Heat map of the time averaged order parameter $\langle r \rangle$ showing the phase transitions promoted by the bifurcation lines.

Figure 1(a) also shows a grid with 8 selected points: four with $\Omega = 0.2$ and four with $\Omega = 1$. Plots of vector fields for these points in the $x = r \cos \psi$ and $y = r \sin \psi$ plane are shown in Figure 2, illustrating how limit cycles and fixed points evolve as F and Ω change for fixed $K_1 = 1$ and $K_{23} = 7$. Panels (a)-(d) have $\Omega = 0.2$ and (e)-(h) have $\Omega = 1$. Panels (d) and (h) for $F = 0.02$ and $F = 0.3$ respectively, show bi-stability: a vanishing order parameter, $r = 0$, is a stable fixed point, but there is also a stable limit cycle with large r and an unstable cycle between these two. The outer cycle represents mutual entrainment, since we are in the frame that rotates with the external force.

Increasing F , panel (c) for $\Omega = 0.2$ and $F = 0.17$, shows that the unstable limit cycle has gone through a SNIPER bifurcation whereas in panel (g), for $\Omega = 1$ and $F = 0.8$, the unstable limit cycle has collided with the origin in a sub-critical Hopf bifurcation, where the origin becomes unstable. Only the external limit cycle is now stable.

Increasing F even more, for $\Omega = 0.2$ and $F = 0.3$, panel (b), two new bifurcations have occurred with respect to $F = 0.17$: a SNIPER in the outer limit cycle and a saddle-node involving the origin and one of the points created at the SNIPER of the old unstable cycle. Three fixed points remain: one stable and one unstable from the SNIPER and another unstable point. For $\Omega = 1$ and $F = 0.99$, panel (f), we see the same structure, although the two unstable points are very close to each other and will soon disappear in another

saddle-node bifurcation.

Finally, panels (a) and (e) for large F shows a single stable point corresponding to forced entrainment.

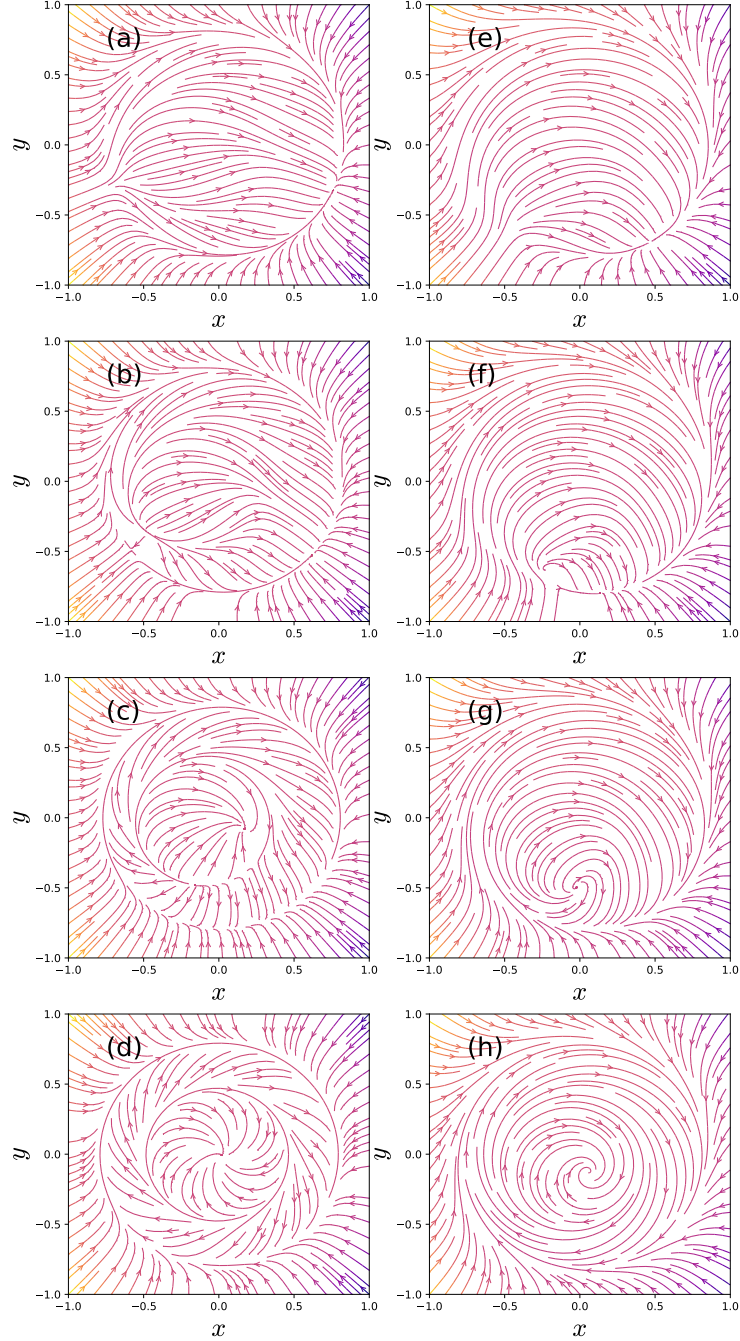


Figure 2. Vector fields for the 8 red points in figure 1. Panels (a) to (d) have $\Omega = 0.2$ and F equal to 0.5, 0.3, 0.17 and 0.02 respectively. Panels (e) to (h) have $\Omega = 1.0$ and F equal to 0.3, 0.8, 0.99 and 1.2 respectively.

D. Evolution of Bifurcation curves

As K_1 and K_{23} varies, the bifurcation manifolds change. For the sake of simplicity we shall refer to the two saddle-node branches as the *green* (thick green line) and *black* (thin black line) branches, referring to the colors displayed in Fig. 1. Figure 3 shows saddle-node and Hopf bifurcation curves in the $F \times \Omega$ plane for a few selected values of K_1 and K_{23} . For $K_1 = 1$, panels (a)-(c), the green branch of the saddle-node manifold is almost independent of K_{23} , whereas the black branch, created for $K_{23} \approx 5.83$ (see below), grows as K_{23} increases. For $K_{23} = 5.8$, panel (a), the black branch has collapsed into the green branch, but its Takens-Bogdanov point remains with its associated Hopf curve. Panels (d)-(f) have $K_{23} = 7$ and increasing values of K_1 . The green branch now shrinks and disappears at $K_1 = 2$. For $K_1 > 2$ only one branch and its attached Hopf curve survive, similar to the case $K_{23} = 0$.

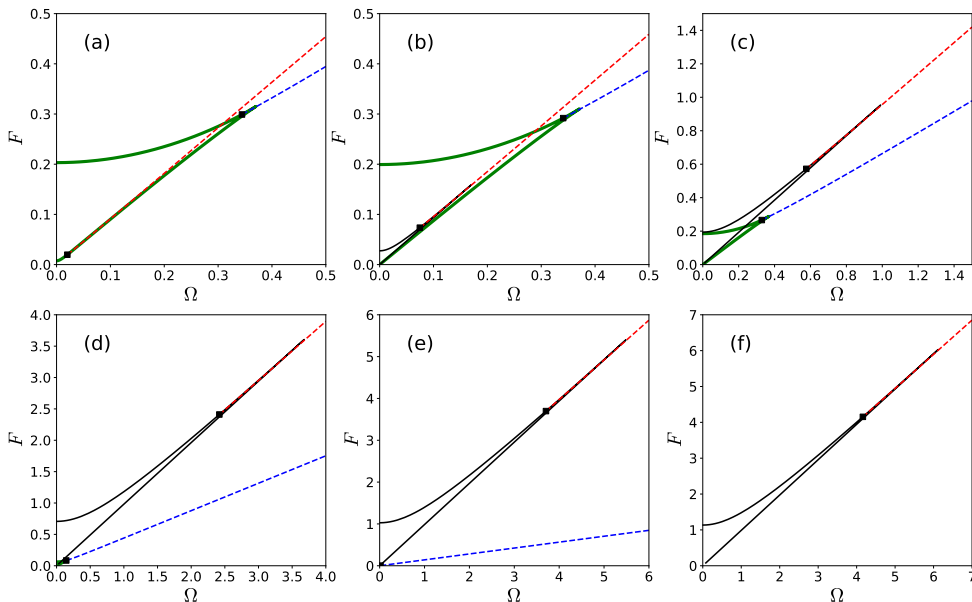


Figure 3. Saddle-node (solid) and Hopf (dashed) curves for different values of K_1 and K_{23} . In panels (a)-(c) $K_1 = 1$ and K_{23} is 5.80, 5.93 and 6.5 respectively. Notice that the thick green saddle-node branch and its correspondent Hopf curve are almost independent of K_{23} , whereas the other ones grow as K_{23} increases. In (d)-(f) $K_{23} = 7$ and K_1 is 1.5, 1.95 and 2.1 respectively. The thick branch disappears at $K_1 = 2$. Black squares show Takens-Bogdanov points.

More information about the critical values described above can be obtained by setting $F = \Omega = 0$ in Eqs. (15) and (16). This amounts to set $A = 0$, Eq.(18). Solving for K_{23} we find $K_{23} = (a - K_1)/r^2$. Imposing $\partial K_{23}/\partial r = 0$ at $r = r_c$ we obtain

$$r_c = 1 - \frac{2}{K_1} + \frac{2}{K_1} \sqrt{1 - \frac{K_1}{2}}. \quad (27)$$

For $K_1 = 1$ we find $r_c = \sqrt{2} - 1$ and $K_{23}(r_c) \approx 5.83$. Below this point the two legs of the black branch collapse into the lower end of the green branch (see Fig. 3(a)). Notice that $K_{23}(r_c)$ is larger than $K_{23}^* \approx 5.306$, which means that two Hopf bifurcation curves exists

attached to a single SN tongue. This phenomena will occur for $K_1 = 1$ as long as K_{23} is lying in $[5.306, 5.83]$ interval. Decreasing K_{23} even more would show the two Takens-Bogdanov points coalescing at K_{23}^* and the Hopf curves disappearing.

Finally, we see that $K_1 = 2$ is also a critical point, where $r_c = 0$ and the green branch disappears. The two branches coexist only for $K_1 < 2$ and $K_{23} > K_{23}(r_c)$.

IV. FORCING PARAMETERS AS FIXED

Now we consider F and Ω as given fixed parameters and vary the coupling parameters K_1 and K_{23} . Our calculations are similar to the ones done in [40], which considered only the case $F = \Omega = 0$.

The authors of [40] found a pitchfork bifurcation for $K_1 = 2$, independent of K_{23} , and a saddle-node bifurcation along a certain curve in the $K_1 \times K_{23}$ plane. It turns out that the situation in the presence of forcing is quite different: for any finite value of the forcing parameters, the pitchfork bifurcation is replaced by another saddle-node curve; moreover, a manifold of Hopf bifurcations also appears.

In this case, by solving the saddle-node conditions $a(r_0, \psi_0) = 0$, $b(r_0, \psi_0) = 0$ and $\det[J(r_0, \psi_0)] = 0$ for K_1 , K_{23} and ϕ , we get the parametric solutions

$$K_{1,\text{SN}} = -\frac{3F^2(1+r^2)}{2Dr} + \frac{4\Omega^2r(1+2r^2)}{D(1+r^2)^2} + \frac{2(1-2r^2)}{(1-r^2)^2}, \quad (28)$$

$$K_{23,\text{SN}} = \frac{F^2(1+r^2)}{2Dr^3} - \frac{4\Omega^2r}{D(1+r^2)^2} + \frac{2}{(1-r^2)^2}, \quad (29)$$

$$\tan(\psi_{\text{SN}}) = \frac{2\Omega r}{D} \quad (-\pi < \psi_{\text{SN}} < 0), \quad (30)$$

where

$$D = \pm\sqrt{F^2(1+r^2)^2 - 4\Omega^2r^2}, \quad (31)$$

with the plus and minus solutions generating two different branches of the bifurcation curve.

For the Hopf bifurcation, on the other hand, it is the trace of the Jacobian that vanishes, instead of the determinant. This leads to

$$K_{1,\text{Hopf}} = \frac{2(1-2r^2)}{(1-r^2)^2} + \frac{D(2-r^2)}{r(1-r^4)}, \quad (32)$$

$$K_{23,\text{Hopf}} = \frac{2}{(1-r^2)^2} - \frac{D}{r^3(1-r^4)}, \quad (33)$$

$$\tan(\psi_{\text{Hopf}}) = \frac{2\Omega r}{D} \quad (-\pi < \psi_{\text{Hopf}} < 0), \quad (34)$$

where again we have two branches.

The determinant of the Jacobian must be positive at the Hopf manifold, which happens to one side of a Takens-Bogdanov point. To find such a point, we must solve $\dot{r} = \dot{\psi} = \text{Tr}(J) = \det(J) = 0$, simultaneously. We find that the easiest way to do this is to treat $\cos \psi$ and $\sin \psi$ as formally independent, solve for $K_1, K_{23}, \cos \psi, \sin \psi$, and then impose $\sin^2 \psi + \cos^2 \psi = 1$, as done in [14]. For given values of (F, Ω) , the value of r which corresponds to the Takens-Bogdanov point satisfies

$$F^2(1 + r_{\text{TB}}^2)^4 = 8\Omega^2 r_{\text{TB}}^2(1 + r_{\text{TB}}^4), \quad (35)$$

and its coordinates in the $K_1 \times K_{23}$ plane are given by (32) and (33) computed at r_{TB} .

Since $r^2(1 + r^4)/(1 + r^2)^4 \leq 1/8$ for $0 \leq r \leq 1$, the above equation only has relevant solutions if $F \leq \Omega$. In general, each Hopf branch has its TB point, and the values of ϕ_{TB} at these different points are related by $\psi_{\text{TB}}^{(2)} = \pi - \psi_{\text{TB}}^{(1)}$.

In Figure 4 we show the bifurcation curves in the $K_1 \times K_{23}$ plane, for a few values of F and Ω . In panels (a)-(e), $\Omega = 0.5$ and F takes the values 0.45, 0.47, 0.49, 0.499 and 0.59, respectively. Initially, we have the saddle-node branches (thin black and thick green solid lines) in some sense connected by the Hopf branches (red and blue dashed lines). The point where the Hopf curves join is K_{23}^* , as discussed in section III B. As F grows, the lower SN branch grows and crosses the upper one, which slowly recedes to negative values of K_1 . When $F \rightarrow \Omega$, the TB points slide off to infinity. In panel (f) we show that for small values of F and Ω , the bifurcation diagram from [40] is recovered.

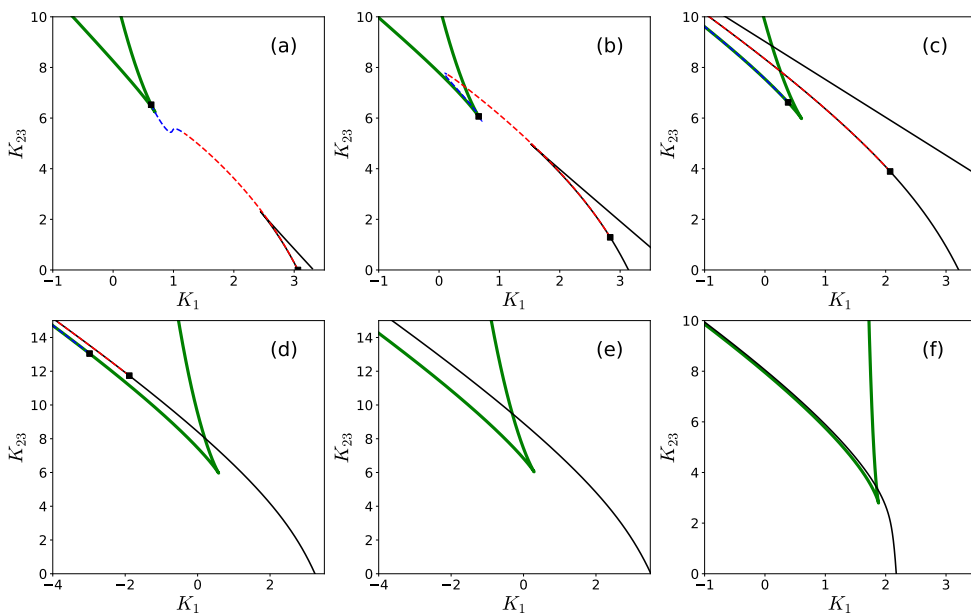


Figure 4. Saddle-node and Hopf curves for different values of F and Ω . In panels (a)-(e) $\Omega = 0.5$ and F is 0.45, 0.47, 0.49, 0.499 and 0.59, respectively. In panel (f), $\Omega = 0.01$ and $F = 0.02$. Black squares show Takens-Bogdanov points.

Figure 5 shows a heat map of the time averaged order parameter $\langle r \rangle$, along with the bifurcation lines. The transitions in this case are not as abrupt as they appear in Figure 1-(b), with the exception of one of them, in the upper branch of the saddle-node manifold.

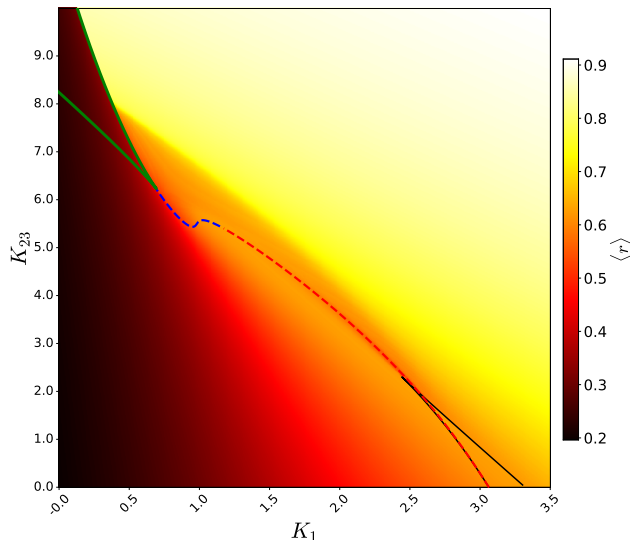


Figure 5. Heat map of the time averaged order parameter $\langle r \rangle$ showing the phase transitions promoted by the bifurcation lines, for $\Omega = 0.5$ and $F = 0.45$, as in fig. 4a.

The Hopf bifurcations, on the other hand, are not very noticeable, because in this case what happens is that a stable fixed point with $\langle r \rangle > 0$ becomes unstable and a periodic orbit is created which has approximately the same $\langle r \rangle$.

V. CONCLUSIONS

In this work we extended the bifurcation analysis of the forced Kuramoto model [14] to the case of asymmetric higher order interactions, as discussed in [40]. We have described in detail how these type of higher order interactions impact the bifurcation diagram obtained originally in [14] in the $F \times \Omega$ plane and also how the intensity and frequency of the external force change the diagram described in [40] in the $K_1 \times K_{23}$ plane.

We have shown that two branches of the saddle-node (SN) bifurcation manifold can co-exist for some values of the parameters, reflecting the bi-stability of the unforced case. From each branch a line of Hopf bifurcation issues from the Takens-Bogdanov (TB) point, dividing the space of parameters in many regions of quite distinct dynamical character, as illustrated in Figs. 1-4.

We did not compute the manifold of homoclinic bifurcations that starts at the TB point and ends at the lower end of the SN tongues [14]. There is no known algebraic procedure to compute these manifolds, i.e. they must be found by numerically scanning the periodic orbits in the vicinity of the cusp of the SN curves, requiring intense numerical calculations.

We note that higher order interactions can be defined in different ways [39–41] and most of them are not amenable to exact treatment under the Ott-Antonsen ansatz. Symmetric interactions, for instance, can lead to multi-stability [39, 41] which could lead to a proliferation of branches in the bifurcation manifolds. We leave the exploration of these cases for future work. Finally, we emphasize that the importance of understanding forced systems of

oscillators goes much beyond pure mathematical interest, and has applications in biological systems such as neurons subjected to visual stimuli, artificial pacemakers for the heart and the circadian rhythms promoted by the day-night cycle.

ACKNOWLEDGMENTS

This work was partly supported by FAPESP, grants 2021/14335-0 (MAMA), 2023/03917-4 (GSC) and 2023/15644-2 (MN), and also by CNPq, grants 301082/2019-7 (MAMA) and 304986/2022-4 (MN).

-
- [1] Y. Kuramoto, "Self-entrainment of a population of coupled non-linear oscillators," in *International Symposium on Mathematical Problems in Theoretical Physics*, pp. 420–422, Berlin/Heidelberg: Springer-Verlag, 1975.
- [2] A. T. Winfree, "Biological rhythms and the behavior of populations of coupled oscillators," *Journal of theoretical biology*, vol. 16, no. 1, pp. 15–42, 1967.
- [3] A. Pikovsky and M. Rosenblum, "Dynamics of globally coupled oscillators: Progress and perspectives," *Chaos: An Interdisciplinary Journal of Nonlinear Science*, vol. 25, no. 9, 2015.
- [4] B. Monga, D. Wilson, T. Matchen, and J. Moehlis, "Phase reduction and phase-based optimal control for biological systems: a tutorial," *Biological cybernetics*, vol. 113, no. 1, pp. 11–46, 2019.
- [5] F. A. Rodrigues, T. K. D. M. Peron, P. Ji, and J. Kurths, "The Kuramoto model in complex networks," *Physics Reports*, vol. 610, pp. 1–98, 2016.
- [6] H. Sakaguchi and Y. Kuramoto, "A soluble active rotator model showing phase transitions via mutual entertainment," *Progress of Theoretical Physics*, vol. 76, no. 3, pp. 576–581, 1986.
- [7] J. Gomez-Gardenes, S. Gomez, A. Arenas, and Y. Moreno, "Explosive synchronization transitions in scale-free networks," *Physical Review Letters*, vol. 106, no. 12, pp. 1–4, 2011.
- [8] P. Ji, T. K. D. Peron, P. J. Menck, F. A. Rodrigues, and J. Kurths, "Cluster explosive synchronization in complex networks," *Physical Review Letters*, vol. 110, no. 21, pp. 1–5, 2013.
- [9] J. S. Climaco and A. Saa, "Optimal global synchronization of partially forced kuramoto oscillators," *Chaos: An Interdisciplinary Journal of Nonlinear Science*, vol. 29, no. 7, p. 073115, 2019.
- [10] S. Chandra, M. Girvan, and E. Ott, "Continuous versus discontinuous transitions in the d-dimensional generalized kuramoto model: Odd d is different," *Physical Review X*, vol. 9, no. 1, p. 011002, 2019.
- [11] M. Lipton, R. Mirollo, and S. H. Strogatz, "On higher dimensional generalized kuramoto oscillator systems," *arXiv preprint arXiv:1907.07150*, 2019.
- [12] A. E. D. Barioni and M. A. de Aguiar, "Ott–antonson ansatz for the d-dimensional kuramoto model: A constructive approach," *Chaos: An Interdisciplinary Journal of Nonlinear Science*, vol. 31, no. 11, p. 113141, 2021.
- [13] R. Fariello and M. A. de Aguiar, "Exploring the phase diagrams of multidimensional kuramoto models," *Chaos, Solitons & Fractals*, vol. 179, p. 114431, 2024.
- [14] L. M. Childs and S. H. Strogatz, "Stability diagram for the forced Kuramoto model," *Chaos*, vol. 18, no. 4, pp. 1–9, 2008.
- [15] C. A. Moreira and M. A. de Aguiar, "Global synchronization of partially forced kuramoto oscillators on networks," *Physica A: Statistical Mechanics and its Applications*, vol. 514, pp. 487–496, 2019.
- [16] C. A. Moreira and M. A. de Aguiar, "Modular structure in c. elegans neural network and its response to external localized stimuli," *Physica A: Statistical Mechanics and its Applications*, vol. 533, p. 122051, 2019.
- [17] G. F. Harding and P. M. Jeavons, *Photosensitive epilepsy*. No. 133, Cambridge University Press, 1994.
- [18] J. B. Reece, *Campbell biology : concepts & connections*. San Francisco, CA.: Benjamin Cummings, 2012.
- [19] A. Pikovsky, M. Rosenblum, and J. Kurths, "Synchronization: A Universal Concept in Nonlinear Sciences," *Cambridge Nonlinear Science Series 12*, p. 432, 2003.
- [20] C. M. Gray, "Synchronous Oscillations in Neuronal Systems: Mechanisms and Functions,"

- Journal of Computational Neuroscience*, vol. 1, pp. 11–38, 1994.
- [21] H. Sakaguchi, “Cooperative phenomena in coupled oscillator systems under external fields,” *Progress of Theoretical Physics*, vol. 79, no. 1, pp. 39–46, 1988.
- [22] E. Ott and T. M. Antonsen, “Low dimensional behavior of large systems of globally coupled oscillators,” *Chaos*, vol. 18, no. 3, pp. 1–6, 2008.
- [23] J. Hindes and C. R. Myers, “Driven synchronization in random networks of oscillators,” *Chaos: An Interdisciplinary Journal of Nonlinear Science*, vol. 25, no. 7, p. 073119, 2015.
- [24] F. Battiston, G. Cencetti, I. Iacopini, V. Latora, M. Lucas, A. Patania, J.-G. Young, and G. Petri, “Networks beyond pairwise interactions: Structure and dynamics,” *Physics Reports*, vol. 874, pp. 1–92, 2020.
- [25] E. Ganmor, R. Segev, and E. Schneidman, “Sparse low-order interaction network underlies a highly correlated and learnable neural population code,” *Proceedings of the National Academy of sciences*, vol. 108, no. 23, pp. 9679–9684, 2011.
- [26] G. Petri, P. Expert, F. Turkheimer, R. Carhart-Harris, D. Nutt, P. J. Hellyer, and F. Vaccarino, “Homological scaffolds of brain functional networks,” *Journal of The Royal Society Interface*, vol. 11, no. 101, p. 20140873, 2014.
- [27] C. Giusti, E. Pastalkova, C. Curto, and V. Itskov, “Clique topology reveals intrinsic geometric structure in neural correlations,” *Proceedings of the National Academy of Sciences*, vol. 112, no. 44, pp. 13455–13460, 2015.
- [28] M. W. Reimann, M. Nolte, M. Scolamiero, K. Turner, R. Perin, G. Chindemi, P. Dłotko, R. Levi, K. Hess, and H. Markram, “Cliques of neurons bound into cavities provide a missing link between structure and function,” *Frontiers in computational neuroscience*, vol. 11, p. 266051, 2017.
- [29] A. E. Sizemore, C. Giusti, A. Kahn, J. M. Vettel, R. F. Betzel, and D. S. Bassett, “Cliques and cavities in the human connectome,” *Journal of computational neuroscience*, vol. 44, pp. 115–145, 2018.
- [30] J. Grilli, G. Barabás, M. J. Michalska-Smith, and S. Allesina, “Higher-order interactions stabilize dynamics in competitive network models,” *Nature*, vol. 548, no. 7666, pp. 210–213, 2017.
- [31] R. Ghosh, U. K. Verma, S. Jalan, and M. D. Shrimali, “Chimeric states induced by higher-order interactions in coupled prey–predator systems,” *Chaos: An Interdisciplinary Journal of Nonlinear Science*, vol. 34, no. 6, 2024.
- [32] A. Sanchez-Gorostiaga, D. Bajić, M. L. Osborne, J. F. Poyatos, and A. Sanchez, “High-order interactions distort the functional landscape of microbial consortia,” *PLoS Biology*, vol. 17, no. 12, p. e3000550, 2019.
- [33] A. R. Benson, D. F. Gleich, and J. Leskovec, “Higher-order organization of complex networks,” *Science*, vol. 353, no. 6295, pp. 163–166, 2016.
- [34] G. F. de Arruda, G. Petri, and Y. Moreno, “Social contagion models on hypergraphs,” *Physical Review Research*, vol. 2, no. 2, p. 023032, 2020.
- [35] I. Iacopini, G. Petri, A. Barrat, and V. Latora, “Simplicial models of social contagion,” *Nature communications*, vol. 10, no. 1, p. 2485, 2019.
- [36] B. Jhun, M. Jo, and B. Kahng, “Simplicial sis model in scale-free uniform hypergraph,” *Journal of Statistical Mechanics: Theory and Experiment*, vol. 2019, no. 12, p. 123207, 2019.
- [37] Y. M. Vega, M. Vázquez-Prada, and A. F. Pacheco, “Fitness for synchronization of network motifs,” *Physica A: Statistical Mechanics and its Applications*, vol. 343, pp. 279–287, 2004.
- [38] V. Bercé, “Chimera state and route to explosive synchronization,” *Chaos, Solitons & Fractals*, vol. 86, pp. 75–81, 2016.
- [39] P. S. Skardal and A. Arenas, “Abrupt desynchronization and extensive multistability in globally

- coupled oscillator simplexes,” *Physical review letters*, vol. 122, no. 24, p. 248301, 2019.
- [40] P. S. Skardal and A. Arenas, “Higher order interactions in complex networks of phase oscillators promote abrupt synchronization switching,” *Communications Physics*, vol. 3, no. 1, p. 218, 2020.
- [41] X. Dai, K. Kovalenko, M. Molodyk, Z. Wang, X. Li, D. Musatov, A. Raigorodskii, K. Alfaro-Bittner, G. Cooper, G. Bianconi, *et al.*, “D-dimensional oscillators in simplicial structures: odd and even dimensions display different synchronization scenarios,” *Chaos, Solitons & Fractals*, vol. 146, p. 110888, 2021.
- [42] B. Moyal, P. Rajwani, S. Dutta, and S. Jalan, “Rotating clusters in phase-lagged kuramoto oscillators with higher-order interactions,” *Phys. Rev. E*, vol. 109, p. 034211, Mar 2024.
- [43] D. Biswas and S. Gupta, “Symmetry-breaking higher-order interactions in coupled phase oscillators,” *Chaos, Solitons & Fractals*, vol. 181, p. 114721, 2024.
- [44] M. Sayeed Anwar, D. Ghosh, and T. Carletti, “Global synchronization on time-varying higher-order structures,” *Journal of Physics: Complexity*, vol. 5, no. 1, p. 015020, 2024.
- [45] R. Muolo, T. Njougouo, L. V. Gambuzza, T. Carletti, and M. Frasca, “Phase chimera states on nonlocal hyperrings,” *Physical Review E*, vol. 109, no. 2, p. L022201, 2024.